

CHEMISTRY

A European Journal

A Journal of



Accepted Article

Title: Computational Characterization of the Mechanism for the Oxidative Coupling of Benzoic Acid and Alkynes by Rh/Cu and Rh/Ag Systems

Authors: Ignacio Funes-Ardoiz and Feliu Maseras

This manuscript has been accepted after peer review and appears as an Accepted Article online prior to editing, proofing, and formal publication of the final Version of Record (VoR). This work is currently citable by using the Digital Object Identifier (DOI) given below. The VoR will be published online in Early View as soon as possible and may be different to this Accepted Article as a result of editing. Readers should obtain the VoR from the journal website shown below when it is published to ensure accuracy of information. The authors are responsible for the content of this Accepted Article.

To be cited as: *Chem. Eur. J.* 10.1002/chem.201800627

Link to VoR: <http://dx.doi.org/10.1002/chem.201800627>

Supported by
ACES

WILEY-VCH

Computational Characterization of the Mechanism for the Oxidative Coupling of Benzoic Acid and Alkynes by Rh/Cu and Rh/Ag Systems

Ignacio Funes-Ardoiz,^{*,[a]} and Feliu Maseras^[a,b]

Abstract: DFT calculations are applied to the study of the oxidative coupling between benzoic acid and 1-phenyl-1-propyne catalyzed by $[\text{CpRhCl}_2]_2$ using either $\text{Cu}(\text{OAc})_2(\text{H}_2\text{O})$ or $\text{Ag}(\text{OAc})$ as terminal oxidants, a process that has been experimentally shown to have subtleties related to regioselectivity (placement of the phenyl substituent of the alkyne in the isocoumarin product) and chemoselectivity (isocoumarin or naphthalene derivatives). Calculations reproduce the experimental results, and show the involvement of the oxidant throughout the catalytic cycle. The regioselectivity is decided in the alkyne insertion step, in particular by the relative arrangement between two phenyl groups. The high chemoselectivity towards isocoumarin associated to $\text{Cu}(\text{OAc})_2(\text{H}_2\text{O})$ is explained because the copper moiety blocks the CO_2 extrusion pathway that would lead to naphthalene derivatives, something that does not happen when $\text{Ag}(\text{OAc})$ is used.

Introduction

Oxidative coupling has emerged in the last years as a powerful approach to build complexity in organic synthesis.¹ Contrary to classical cross-coupling alternatives (*i.e.* Suzuki-Miyaura, Negishi, etc.), this methodology does not require prefunctionalization of the substrate, allowing the direct activation of C-H bonds. This complements the cross-coupling reaction scope and converts oxidative coupling into a promising alternative for new reaction designs, especially to build new C-C or C-X (X = heteroatom) bonds. The general scheme is that a transition metal in high oxidation state activates the substrate (usually a C-H bond) and then the C-X bond is formed by reductive elimination. Oxidative coupling differs from cross-coupling in that the two reactants are oxidized during the reaction and thus an external oxidant is needed to close the catalytic cycle. Different metal catalysts and oxidants have been extensively used during the last years for this process. A particular successful set is defined by the reactions based on rhodium,² palladium,³ ruthenium⁴ catalysts that employ copper diacetate⁵ or silver acetate⁶ as final oxidant. Recently, non-noble metals such as copper⁷ and cobalt⁸ have been also used as a cheaper alternative, but the performance is still far from that of

precious metals. Alternative oxidants like Oxone can be also used,⁹ but are less common. There are examples in which molecular oxygen can be used as final oxidant,¹⁰ though two co-catalysts, typically Rh(III) and Cu(II)-based, are used in those cases.¹¹

There are a series of diverse experimental data on the reasons why some systems are preferred. The role of an acetate ligand in the oxidant is likely related to its known role as a facilitating agent for the deprotonation of C-H bonds through concerted metalation-deprotonation transition state (CMD).¹² The election of Ag or Cu is still a matter of discussion,¹³ although it can affect the selectivity of the processes. The nature of the active form of the Rh(III)-based catalyst is still unclear. In most reactions, $[\text{CpRhCl}_2]_2$ is used as a precursor and $[\text{CpRh}(\text{OAc})_2]$ is postulated as active species. However, Jones and co-workers analyzed the formation of $[\text{CpRh}(\text{OAc})_2]$, proving that it is formed only at high concentrations of free acetate (NaOAc or CsOAc).¹⁴ Silver species have been used to trap the chloride atoms from the precursor and that is why sometimes catalytic amounts of silver acetate are used even if copper acetate is used as final oxidant.

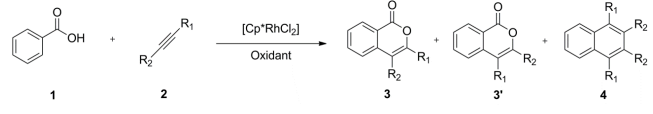
Despite the many experimental advances, the theoretical background of oxidative couplings is still in the early stages,¹⁵ as the substantial advances in catalytic cycles for cross-coupling catalytic cycles,¹⁶ and on metal catalyzed C-H activation¹⁷ have not found full translation yet. The computational study of oxidative coupling has focused mainly on the influence of acetate ligands in the C-H activation step (via CMD transition state).¹⁸ Only some catalytic cycles have been reported in the case of the rhodium catalyzed oxidative couplings, such as internal oxidant-controlled reactions,¹⁹ an intramolecular version of alkyne coupling to a benzamide,²⁰ and a comprehensive study of heterocycle synthesis in which selectivity issues were also addressed.²¹ In these previous works $[\text{CpRh}(\text{OAc})_2]$ was assumed to be the active species, which is not obvious under the presence of copper acetate as oxidant. Recently, a detailed mechanistic study has been carried out in a cobalt catalyzed C-N coupling, but cobalt, as first row transition metal, operates in a variety of spin and oxidation states, differing in this sense from rhodium.^{8b} The effect of the additives in the chemoselectivity of other reactions has been study in related processes²² but is still unexplored for most of the oxidative couplings.

We reported previously a computational study on a specific step, the reductive elimination, of the rhodium catalyzed oxidative coupling between benzoic acid and alkynes.²³ We showed that the copper diacetate dimer oxidant accepts one electron during the reductive elimination, leading to the formation of a Rh(II) intermediate instead of the previously postulated Rh(I) species. We labeled this process as cooperative reductive elimination (CRE). Experimentally, this copper influence has been reported by Patureau and co-workers in the Ru-catalyzed homocoupling of carbazoles.²⁴

[a] Dr. I. Funes-Ardoiz, Prof. Dr. F. Maseras
Institute of Chemical Research of Catalonia
The Barcelona Institute of Science and Technology
Avda. Paisos Catalans 16, 43007 Tarragona (Spain)
E-mail: ifunes@icig.es

[b] Prof. Dr. F. Maseras
Department de Química
Universitat Autònoma de Barcelona
08193 Bellaterra (Spain)

Supporting information for this article is given via a link at the end of the document.

Table 1. Experimental results of the oxidative coupling between benzoic acid and alkynes under different oxidants.²⁵


Oxidant	R ₁	R ₂	Solvent	Temp (°C)	Time (h)	Products: % yield
Cu(OAc) ₂ ·H ₂ O	Ph	Me	<i>o</i> -xylene	120	6	3 : 89; 3' : 9; 4 : 0
Ag(OAc)	Ph	Ph	Mesitylene	180	2	3 = 3' : 40; 4 : 60

In the current manuscript we extend our previous study to the full catalytic cycle for the reaction of benzoic acid with asymmetric alkynes reported by Miura and Satoh (Table 1).^{25,26} We study first the full catalytic cycle of the reaction between 1-phenyl-1-propyne and benzoic acid catalyzed by Rh/Cu combination (entry 1, Table 1), paying special attention to the regioselectivity issues. We analyze later the influence of silver acetate in the chemoselectivity of the reaction (entry 2, Table 1). We expect this study will help in the rational development of new reactions.²⁷

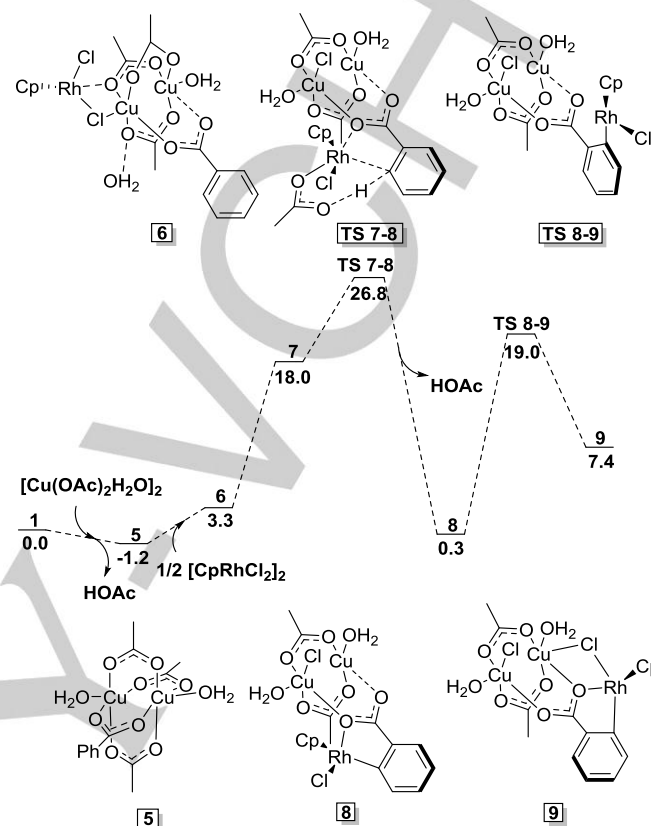
Results and Discussion

1. Full catalytic cycle of oxidative coupling catalyzed by Rh/Cu cooperative system

We started calculating the catalytic cycle using [CpRh(OAc)₂] as the initial catalyst, following the initial proposal from the experimental group. The results are shown in the Supporting Information (Figures S1 and S2) and do not reproduce the experimental chemoselectivity. According to our calculations on this Rh-alone mechanism only the naphthalene derivative product should be formed because the reductive elimination barrier to yield the isocoumarin is 5.0 kcal/mol higher than that leading to the naphthalene derivative. In contrast, only the isocoumarin product is observed experimentally (entry 1, table 1).

We considered next an early involvement of the oxidant in the catalytic cycle. We started the mechanistic study with all the species in solution as the reference point (Figure 1, 1). The copper diacetate dimer can exchange one of the acetate groups by benzoate exergonically (-1.2 kcal/mol). This species binds to the unsaturated monomer [CpRhCl₂], forming adduct **6**. Then, one acetate ligand is exchanged by a chloride ligand in the rhodium center yielding intermediate **7**, which has the appropriate geometry to promote the concerted-metallation-deprotonation (CMD). The C-H activation transition state (**TS 7-8**), has a barrier of 26.8 kcal/mol, which is lower in energy than the previously proposed transition state based on [CpRh(OAc)₂], which was 28.7 kcal/mol above the reactants (see Figure S1 in

the Supporting Information). This is the highest point of the free energy profile, so the C-H activation is the rate determining step.

**Figure 1.** Free energy profile of the C-H activation of benzoic acid by the Rh/Cu cooperative system. Free energies in kcal/mol.

The resulting 5-member rhodacycle **8** is stable (0.3 kcal/mol) and has been proposed and detected in other similar reactions.²⁸ This intermediate evolves to the following intermediate **9** by a dihedral rotation of the aromatic ring through an accessible transition state at 19.0 kcal/mol. In intermediate **9**, there is a chloride bridge between Rh and Cu, which will be important in the reductive elimination step, and gives the complex enough flexibility to coordinate the alkyne in the following steps.

Once the C-H bond has been activated, intermediate **9** can coordinate 1-phenyl-1-propyne in two different ways (Figure 2), with the phenyl group pointing away from (**10**) or towards (**10'**) the benzoate ring. The relative stability of these intermediates is reversed in the associated transition states. The favored evolution goes to intermediate **11**, preferred over **11'** by a barrier difference of 2.5 kcal/mol. This translates to a predicted regioselectivity of 96:4 at 120°C, in reasonable agreement with the experimental outcome (91:9). The overall barrier for the alkyne insertion is 22.7 kcal/mol, lower than that of the C-H activation.

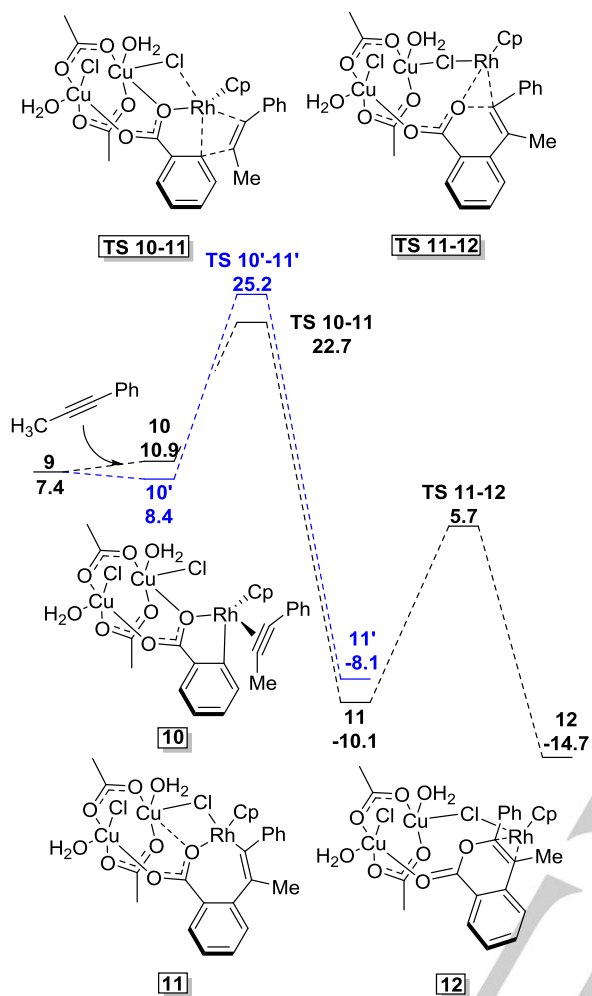


Figure 2. Free energy profile of the alkyne insertion and the reductive elimination steps. Free energies in kcal/mol.

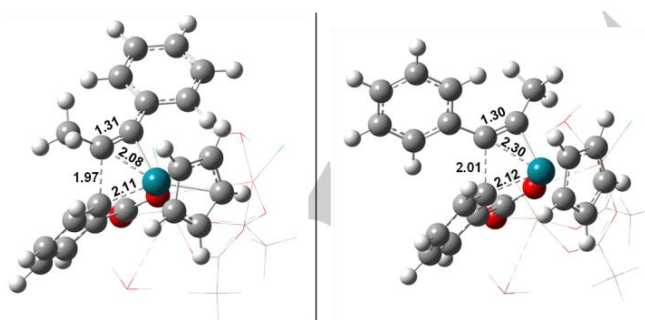


Figure 3. Structures of the alkyne insertion transition states, **TS 10-11** (left) and **TS 10'-11'** (right). Relevant bond distances are depicted in Å.

The phenyl group in the alkyne and its interactions are the key to understand the regioselectivity. In **TS 10-11** (Figure 3, left), the phenyl group is pointing out and there is no steric hindrance with

the rest of the structure, favoring a strong interaction between alkyne carbon and the rhodium center at 2.08 Å. This favors a short distance of 1.97 Å, in the C-C bond that is being formed. However, in **TS 10'-11'**, this phenyl group is hindered by the aromatic ring of the benzoic acid. The interaction is repulsive because the two aromatic groups are perpendicular and no π - π stacking interaction can take place.

The next step is the reductive elimination yielding the isocoumarin compound **3** via cooperative reductive elimination (CRE) with a barrier of 15.8 kcal/mol referred to **11**. This step was the subject of our previous publication on the topic, and will not be discussed in detail here. Two electrons are transferred from the organic reactants to the three metal cluster, one to the rhodium center and the other to the Cu-Cu dimeric system, yielding intermediate **12**, which has an electronic structure with the metals in the oxidation state Rh(II)-Cu(I-II)-Cu(I-II). This CRE is much lower in free energy barrier than the competing barriers in the Rh-alone pathway, where the CO₂ extrusion pathway had the lowest one at 12.2 kcal/mol. The presence of Rh(II) after the reductive elimination is further confirmed here by the analysis of the separation of the Rh moiety from the intermediate **12**, as shown in Figure 4. A Rh(II) fragmentation is much favored over a Rh(I) fragmentation at this point (-0.8 kcal/mol versus +57.6 kcal/mol), which excludes the formation of Rh(I) during the catalytic cycle.

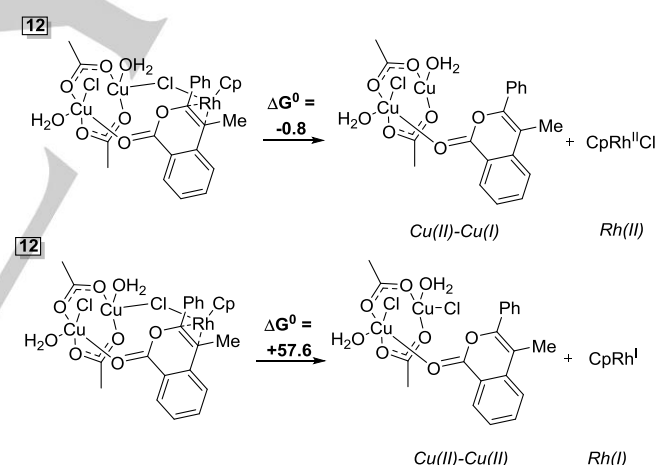


Figure 4. Relative stability of Rh(II) species respect to Rh(I) from intermediate **12**. Free energies in kcal/mol.

The last step in the catalytic cycle is liberation of isocoumarin **3** from this intermediate (Figure S3), which produces **13** exergonically (-27.6 kcal/mol). The singlet state of this intermediate, which corresponds with Rh(III)-Cu(I)-Cu(I) electronic structure, is more stable by 4.1 kcal/mol, regenerating the initial [CpRh(III)Cl₂]₂ species and forming [Cu(OAc)(H₂O)]₂ as side product with an overall exergonicity for the overall process of -39.0 kcal/mol.

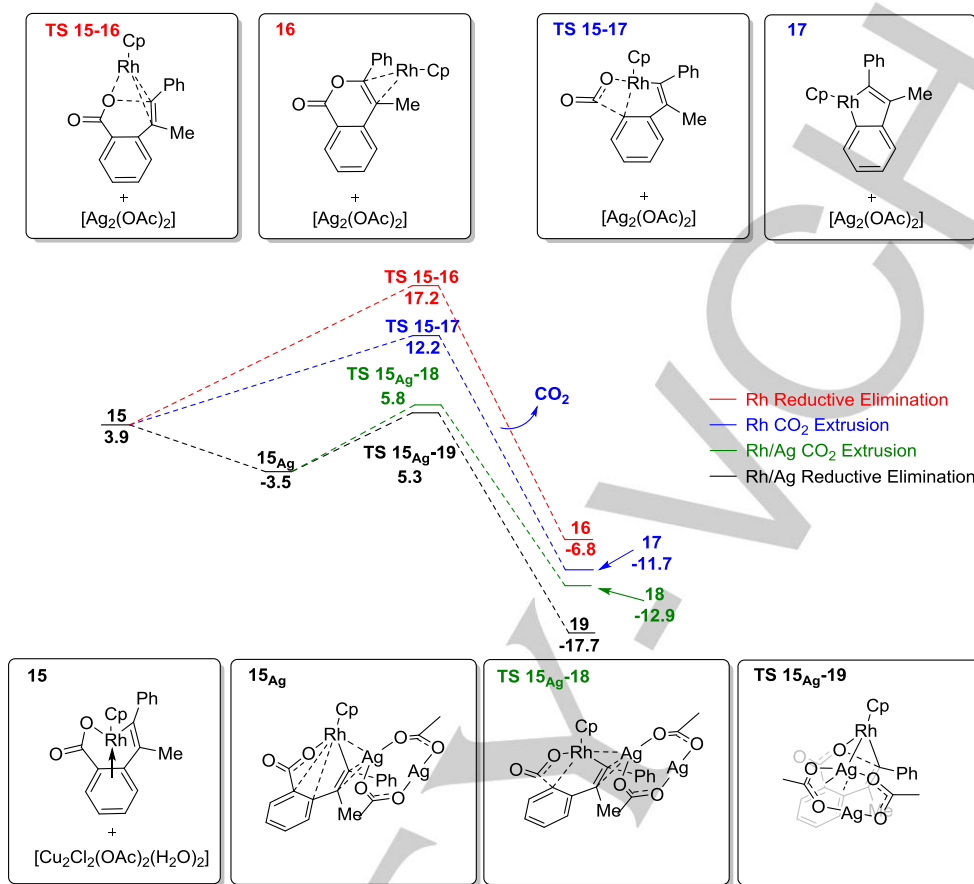


Figure 5. Comparison between the reductive elimination and CO₂ extrusion pathways in Rh catalyzed oxidative coupling with Ag(OAc) as oxidant. Energies in kcal/mol.

2. AgOAc as a terminal oxidant and its influence on the chemoselectivity

As we pointed out in the introduction, silver acetate has been also extensively used in oxidative couplings as final oxidant or as an additive to remove chloride groups from the rhodium precursor. Silver acetate is an even better oxidant than copper diacetate and one could expect a similar behavior, but this is not the case in general. In this specific oxidative coupling of benzoic acid and alkyne, the oxidant affects considerably the chemoselectivity of the process. When AgOAc is used (entry 2, Table 1), the chemoselectivity of the reaction drops down, yielding 40 % of the isocoumarin compound and 60% of the naphthalene derivative product. Here, we analyze computationally the effect of the change of oxidant in the reductive elimination step. For comparative reasons we keep the temperature, 1-phenyl-1-propyne as the substrate and *o*-xylene as the solvent, although the experiment was reported using 180°C, diphenylacetylene and mesitylene, respectively. It is well known, that silver can trap the chloride atoms of the rhodium precatalyst, favoring the formation of [CpRh(OAc)₂] as the active species. This would favor the Rh-alone path (Figures

S1 and S2) discussed above, but if this were the case, only the naphthalene product should be obtained because the reductive elimination transition state (TS 15-16) is 5.0 kcal/mol higher than that for CO₂ extrusion (TS 15-17). This corresponds with a predicted product distribution of >99:1, favoring naphthalene (Figure 5, red and blue pathways, respectively).

We evaluated thus the potential involvement of silver acetate in the chemoselectivity-determining transition states. We consider silver acetate as a dimer because the dissociation energy to form the monomer is very high (29.3 kcal/mol) and the reductive elimination assisted by Ag(OAc) as a monomer has an energy of 18.1 kcal/mol, higher than Rh alone pathway TSs. Silver acetate can indeed cooperate as a dimer in both transition states (Figure 5, green and black pathways). The reductive elimination (TS 15_{Ag}-19) is also favored (as in copper cooperative pathway) but this time, the CO₂ extrusion (TS 15_{Ag}-18) is much more competitive. The difference between both transition states is only 0.5 kcal/mol, which corresponds to a ratio of 64:36 at 180°C favoring the isocoumarin product. This value is comparable with the experimental value of 40:60 when diphenylacetylene is used, and shows a clear qualitative difference with the copper systems.

In addition, both transition states are remarkably lower than the Rh-alone pathways (blue and red in Figure 5), demonstrating that cooperative effects might be also present when silver is used as oxidant in other reactions. The structures of all the transition states are shown in figure S4 in the Supporting Information.

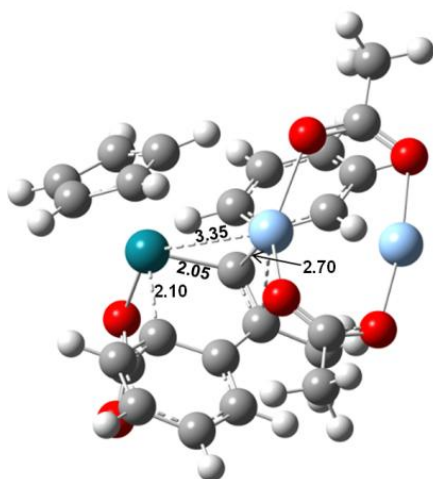


Figure 6. Structure of the transition state for the silver mediated CO₂ extrusion (TS 16-18). Relevant bond distances are depicted in Å.

Finally, we analyze the structure of **TS 15_{Ag}-18**, in which silver facilitates the CO₂ extrusion. In this case, silver is strongly coordinated to the C=C bond in the structure (2.70 Å) and interacts also with the rhodium center (3.35 Å). The pseudoplanar structure of silver acetate allows the structure to be in this conformation, stabilizing the CO₂ extrusion by 6.6 kcal/mol respect **TS 15-17**. This transition state cannot be found when copper(II) acetate acts as an oxidant due to the bulkier structure of the dimer, with four bridging acetate groups which prevent the favorable C=C interaction with copper centers.

Conclusions

Density Functional Theory (DFT) has been used to describe the full catalytic cycle of the rhodium-catalyzed oxidative coupling between benzoic acid and alkynes. The reaction is complex, but all the experimental data are reproduced, which confirms computational chemistry to be a useful tool to understand the process and build a complete mechanistic picture, facilitating the rational design of new reactions.

Two key aspects were analyzed in detail: the regioselectivity of the alkyne insertion and the chemoselectivity of the process. The first one is found to be due to the steric hindrance of the phenyl groups of both reactants, benzoic acid and 1-phenyl-1-propyne, which stabilize the transition state with both phenyl groups far from each other. The chemoselectivity is shown to be strongly correlated to the identity of the oxidant employed in the reaction. If copper diacetate is used, its presence blocks

effectively the CO₂ extrusion and stabilizes the reductive elimination through cooperative effect between copper centers and rhodium, producing favorably the isocoumarin product. In contrast, when silver acetate is used, the planar structure of silver acetate dimer does not block the CO₂ extrusion, allowing a competition between two different pathways, and forming isocoumarin and naphthalene derivative products in similar yields.

The cooperation of different metals throughout the oxidative coupling mechanism is thus found to be relevant for both the Rh/Cu and Rh/Ag systems. This suggests oxidant involvement may be also present in the mechanism for other systems, and hints to new approaches to the development of efficient oxidative coupling processes.

Computational Details

All calculations were carried out with the Gaussian09 package (version D.01)²⁹ using density functional theory. All the energies reported in the main text were obtained with the B97D functional.³⁰ Additional benchmark calculations were reported with other functionals in our previous work,²³ demonstrating the good performance of B97D. Solvation was considered implicitly in all cases through the SMD model,³¹ using the experimental solvent, o-xylene, as the model solvent ($\epsilon = 2.5454$). All the reported geometry optimizations were carried out without symmetry restriction and the number of imaginary frequencies as checked, zero for minima and one for transition states. IRC calculations were also done when the connectivity of the reactants and products through a transition state was not clear enough.

We used two basis sets, one for optimizations and frequency calculations (Basis set I) and the other for refining the potential energies through single point calculations (Basis set II). Basis Set I was LANL2DZ³² for rhodium and copper atoms (with the associated pseudopotentials) and 6-31G(d) for other atoms.³³ Basis set II was LANL2TZ(f)³⁴ for Rh and Cu and 6-311++G(d,p) for the remaining atoms.³⁵ Free energy corrections were initially calculated at 298.15 K temperature and 101325 Pa pressure, including zero point energy corrections (ZPE). The temperature was then changed to 393.15 K and the reference state to 1 M using the freely available GoodVibes script.³⁶ All reported energies in the text correspond to free energies in solution, calculated from potential energies with basis set II plus free energy corrections obtained with basis set I at the geometry of the optimization with basis set I. The Cp* ligand was replaced by Cp to reduce the computational cost.

A dataset collection of computational results is available in the ioChem-BD repository.³⁷

Acknowledgements

We thank for financial support the CERCA Programme / Generalitat de Catalunya and MINECO (Grants CTQ-2017-87792-R and Severo Ochoa Excellence Accreditation 2014-2018 SEV-2013-0319) and . I.F.-A thanks the Severo Ochoa predoctoral training fellowship (Ref: SVP-2014-068662).

Keywords: Oxidative Coupling • Density Functional Theory • Mechanism • Oxidant Effect • Chemoselectivity

- [1] A. Lei, W. Shi, C. Liu, W. Liu, H. Zhang, C. He in *Oxidative Cross-Coupling Reactions, 1st Edition*, Wiley-VCH, Weinheim, **2017**.
- [2] a) D. A. Colby, A. S. Tsai, R. G. Bergman, J. A. Ellman, *Acc. Chem. Res.* **2012**, *45*, 814-825. b) G. Song, F. Wang, X. Li, *Chem. Soc. Rev.* **2012**, *41*, 3651-3678.
- [3] T. W. Lyons, M. S. Sanford, *Chem. Rev.* **2010**, *110*, 1147-1169.
- [4] P. B. Arockiam, C. Bruneau, P. H. Dixneuf, *Chem. Rev.* **2012**, *112*, 5879-5918.
- [5] a) D. R. Stuart, M. Bertrand-Laperle, K. M. N. Burgess, K. Fagnou, *J. Am. Chem. Soc.* **2008**, *130*, 16474-16475. b) M.-L. Louillat, A. Biafora, F. Legros, F. W. Patureau, *Angew. Chem. Int. Ed.* **2014**, *53*, 3505-3509. c) J. Zheng, S.-B. Wang, C. Zheng, S.-L. You, *J. Am. Chem. Soc.* **2015**, *137*, 4880-4883. d) A. M. Martínez, J. Echavarren, I. Alonso, N. Rodríguez, R. Gómez Arrayás, J. C. Carretero, *Chem. Sci.* **2015**, *6*, 5802-5814.
- [6] a) Y. Du, T. K. Hyster, T. Rovis, *Chem. Commun.* **2011**, *47*, 12074-12076. b) J. M. Neely, T. Rovis, *J. Am. Chem. Soc.* **2013**, *135*, 66-69. c) B. Liu, P. Hu, X. Zhou, D. Bai, J. Chang, X. Li, *Org. Lett.* **2017**, *19*, 2086-2089.
- [7] X.-X. Guo, D.-W. Gu, Z. Wu, W. Zhang, *Chem. Rev.* **2015**, *115*, 1622-1651.
- [8] a) M. Moselage, J. Li, L. Ackermann, *ACS Catal.* **2016**, *6*, 498-525. b) R. Mei, H. Wang, S. Warratz, S. A. Macgregor, L. Ackermann, *Chem. Eur. J.* **2016**, *22*, 6759-6763.
- [9] a) Z.-H. Guan, Z.-H. Ren, S. M. Spinella, S. Yu, Y.-M. Liang, X. Zhang, *J. Am. Chem. Soc.* **2009**, *131*, 729-733. b) A. Iturmendi, M. Iglesias, J. Munárriz, V. Polo, J. J. Pérez-Torrente, L. A. Oro, *Chem. Commun.* **2017**, *53*, 404-407.
- [10] a) G. Zhang, L. Yang, Y. Wang, Y. Xie, H. Huang, *J. Am. Chem. Soc.* **2013**, *135*, 8850-8853. b) S. Warratz, C. Kornhaas, A. Cajaraville, B. Niepötter, D. Stalke, L. Ackermann, *Angew. Chem. Int. Ed.* **2015**, *54*, 5513-5517. c) Z. Shi, C. Zhang, S. Li, D. Pan, S. Ding, Y. Cui, N. Jiao, *Angew. Chem. Int. Ed.* **2009**, *48*, 4572-4576.
- [11] a) A. Biafora, F. W. Patureau, *Synlett* **2014**, *25*, 2525-2530. b) J. A. Leitch, P. B. Wilson, C. L. McMullin, M. F. Mahon, Y. Bhoonah, I. H. Williams, C. G. Frost, *ACS Catal.* **2016**, *6*, 5520-5529.
- [12] a) S. I. Gorelsky, D. Lapointe, K. Fagnou, *J. Am. Chem. Soc.* **2008**, *130*, 10848-10849. b) D. L. Davies, S. A. Macgregor, C. L. McMullin, *Chem. Rev.* **2017**, *117*, 8649-8709.
- [13] F. W. Patureau, J. Wencel-Delord, F. Glorius, *Aldrichimica Acta* **2012**, *45*, 31-41.
- [14] L. Li, W. W. Brennessel, W. D. Jones, *Organometallics* **2009**, *28*, 3492-3500.
- [15] I. Funes-Ardoiz, F. Maseras, *ACS Catal.* **2018**, *8*, 1161-1172.
- [16] M. García-Melchor, A. A. C. Braga, A. Lledós, G. Ujaque, F. Maseras, *Acc. Chem. Res.* **2013**, *46*, 2626-2634.
- [17] a) D. Balcells, E. Clot, O. Eisenstein, *Chem. Rev.* **2010**, *110*, 749-823. b) D. García-Cuadrado, P. de Mendoza, A. A. C. Braga, F. Maseras, A. M. Echavarren, *J. Am. Chem. Soc.* **2007**, *129*, 6880-6886.
- [18] J. Jiang, R. Ramozzi, K. Morokuma, *Chem. Eur. J.* **2015**, *21*, 11158-11164.
- [19] a) L. Xu, Q. Zhu, G. Huang, B. Cheng, Y. Xia, *J. Org. Chem.* **2012**, *77*, 3017-3024. b) N. Semakul, K. E. Jackson, R. S. Paton, T. Rovis, *Chem. Sci.* **2017**, *8*, 1015-1020.
- [20] N. Quiñones, A. Seoane, R. García-Fandiño, J. L. Mascareñas, M. Gulías, *Chem. Sci.* **2013**, *4*, 2874-2879.
- [21] D. L. Davies, C. E. Ellul, S. A. Macgregor, C. L. McMullin, K. Singh, *J. Am. Chem. Soc.* **2015**, *137*, 9659-9669.
- [22] a) M. Anand, R. B. Sunoj, H. F. Schaefer III, *J. Am. Chem. Soc.* **2014**, *136*, 5535-5538. b) Y. Liu, Y. Tang, Y.-Y. Jiang, X. Zhang, P. Li, S. Bi, *ACS Catal.* **2017**, *7*, 1886-1896.
- [23] I. Funes-Ardoiz, F. Maseras, *Angew. Chem. Int. Ed.* **2016**, *55*, 2764-2767.
- [24] M.-L. Louillat, F. W. Patureau, *Org. Lett.* **2013**, *15*, 164-167.
- [25] K. Ueura, T. Satoh, M. Miura, *M. J. Org. Chem.* **2007**, *72*, 5362-5367.
- [26] K. Ueura, T. Satoh, M. Miura, *Org. Lett.* **2007**, *9*, 1407-1409.
- [27] D. Balcells, E. Clot, O. Eisenstein, A. Nova, L. Perrin, *Acc. Chem. Res.* **2016**, *49*, 1070-1078.
- [28] a) L. Li, W. W. Brennessel, W. D. Jones, *J. Am. Chem. Soc.* **2008**, *130*, 12414-12419. b) N. Wang, B. Li, H. Song, S. Xu, B. Wang, *Chem. Eur. J.* **2013**, *19*, 358-364.
- [29] Gaussian 09, Revision D.01, M. J. Frisch, G. W. Trucks, H. B. Schlegel, G. E. Scuseria, M. A. Robb, J. R. Cheeseman, G. Scalmani, V. Barone, G. A. Petersson, H. Nakatsuji, X. Li, M. Caricato, A. Marenich, J. Bloino, B. G. Janesko, R. Gomperts, B. Mennucci, H. P. Hratchian, J. V. Ortiz, A. F. Izmaylov, J. L. Sonnenberg, D. Williams-Young, F. Ding, F. Lipparini, F. Egidi, J. Goings, B. Peng, A. Petrone, T. Henderson, D. Ranasinghe, V. G. Zakrzewski, J. Gao, N. Rega, G. Zheng, W. Liang, M. Hada, M. Ehara, K. Toyota, R. Fukuda, J. Hasegawa, M. Ishida, T. Nakajima, Y. Honda, O. Kitao, H. Nakai, T. Vreven, K. Throssell, J. A. Montgomery, Jr., J. E. Peralta, F. Ogliaro, M. Bearpark, J. J. Heyd, E. Brothers, K. N. Kudin, V. N. Staroverov, T. Keith, R. Kobayashi, J. Normand, K. Raghavachari, A. Rendell, J. C. Burant, S. S. Iyengar, J. Tomasi, M. Cossi, J. M. Millam, M. Klene, C. Adamo, R. Cammi, J. W. Ochterski, R. L. Martin, K. Morokuma, O. Farkas, J. B. Foresman, and D. J. Fox, Gaussian, Inc., Wallingford CT, **2016**.
- [30] S. Grimme, *J. Comp. Chem.* **2006**, *27*, 1787-1799.
- [31] S. A. V. Marenich, C. J. Cramer, D. G. Truhlar, *J. Phys. Chem. B*, **2009**, *113*, 6378-6396.
- [32] P. J. Hay, W. R. Wadt, *J. Chem. Phys.* **1985**, *82*, 270-283.
- [33] a) W. J. Hehre, R. Ditchfield, J. A. Pople, *J. Chem. Phys.* **1972**, *56*, 2257-2261. b) P. C. Hariharan, J. A. Pople, *Theoret. Chimica Acta* **1973**, *28*, 213-222. c) M. M. Francl, W. J. Pietro, W. J. Hehre, J. S. Binkley, M. S. Gordon, D. J. DeFrees, J. A. Pople, *J. Chem. Phys.* **1982**, *77*, 3654-3665.
- [34] L. E. Roy, P. J. Hay, R. L. Martin, *J. Chem. Theory Comput.* **2008**, *4*, 1029-1031.
- [35] a) R. Krishnan, J. S. Binkley, R. Seeger, J. A. Pople, *J. Chem. Phys.* **1980**, *72*, 650-654. b) A. D. McLean, G. S. Chandler, *J. Chem. Phys.* **1980**, *72*, 5639-5648.
- [36] I. Funes-Ardoiz, R. S. Paton Goodvibes, version 1.0.1., DOI: 10.5281/zenodo.595246.
- [37] M. Alvarez-Moreno, C. de Graaf, N. Lopez, F. Maseras, J. M. Poblet, C. Bo, *J. Chem. Inf. Model.* **2015**, *55*, 95-103.

Biographical Sketch



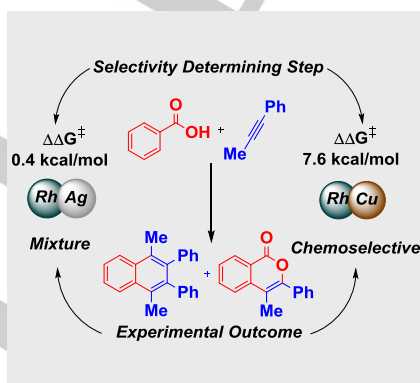
Ignacio Funes-Ardoiz was born in Tudela, Spain, in 1991. He received his Ph.D. from the Institute of Chemical Research of Catalonia (ICIQ) in September, 2017 in the group of F. Maseras. He is temporarily working as postdoctoral researcher in the same group. During the doctoral studies, he worked three months as visiting student in the University of Oxford under the supervision of R. S. Paton. His research is focused on the DFT computational study of homogeneous redox processes, especially on the oxidative coupling reactions and the water oxidation catalysis. In addition, he is involved in different science outreach activities.

Entry for the Table of Contents

Layout 1:

FULL PAPER

Cooperation matters: DFT calculations demonstrate the key role of the oxidant in rhodium-catalyzed oxidative coupling processes. Both copper and silver oxidants interact with rhodium throughout the catalytic cycle, and their involvement explains the regioselectivity and chemoselectivity of the process.



Ignacio Funes-Ardoiz*, Feliu Maseras

Page No. – Page No.

Computational Characterization of the Mechanism for the Oxidative Coupling of Benzoic Acid and Alkynes by Rh/Cu and Rh/Ag Systems